



Xiaodong Xia · George J. Weng  · Juanjuan Zhang · Yang Li

The effect of temperature and graphene concentration on the electrical conductivity and dielectric permittivity of graphene–polymer nanocomposites

Received: 12 August 2019 / Revised: 12 October 2019 / Published online: 1 January 2020
© Springer-Verlag GmbH Austria, part of Springer Nature 2020

Abstract Several recent experiments have revealed the remarkable influence of temperature and graphene concentration on the effective electrical properties of graphene–polymer nanocomposites, but no theory seems to exist at present to quantify such dependence. In this work, we develop a novel micromechanics-based homogenization scheme to connect the microstructural features of constituent phases to the temperature-dependent macroscopic conductivity and permittivity for the nanocomposites. The key microstructural features include the graphene volume concentration, temperature-dependent electrical properties of constituent phases, percolation threshold, imperfect mechanical bonding effect with temperature-degraded interlayer, and the temperature-dependent electron tunneling and Maxwell–Wagner–Sillars polarization. We consider the activation of free electrons and polarization of molecules to write the constitutive equations of polymer, and the collision and vibration probabilities to write those of graphene. We highlight the developed theory with a direct comparison to the experimental data of rGO/epoxy nanocomposites over the temperature range from 293 to 353 K. It shows that before the percolation threshold, the effective electrical conductivity and dielectric permittivity markedly increase with temperature, but after the percolation threshold, the influence of temperature diminishes significantly. In the latter case, the effective permittivity increases only slightly, while the conductivity exhibits an opposite trend.

X. Xia
School of Civil Engineering, Central South University, Changsha 410083, People’s Republic of China

G. J. Weng (✉)
Department of Mechanical and Aerospace Engineering, Rutgers University, New Brunswick, NJ 08903, USA
E-mail: gjweng@soe.rutgers.edu

J. Zhang
Department of Mechanics and Engineering Science, College of Civil Engineering and Mechanics, Lanzhou University, Lanzhou, Gansu 730000, People’s Republic of China

J. Zhang
Key Laboratory of Mechanics on Environment and Disaster in Western China, The Ministry of Education of China, Lanzhou University, Lanzhou, Gansu 730000, People’s Republic of China

Y. Li (✉)
State Key Laboratory of Powder Metallurgy, Central South University, Changsha 410083, People’s Republic of China
E-mail: liyang16@csu.edu.cn

1 Introduction

Low-dimensional functional nanocomposites [1] have been widely utilized in many applications due to their ultra-high electrical conductivity and permittivity. The applications include high efficient batteries [2], energy harvesting and storage systems [3,4], functional sensors [5,6], electromagnetic interference shielding devices [7,8], etc. Typical examples of low-dimensional functional materials are graphene, carbon nanotubes (CNT) and silicene. Graphene is a two-dimensional one-atom-thick layer of sp^2 -bonded carbon atoms with remarkable electrical properties on the basal plane [9]. However, a single-phase graphene nanofiller cannot attain high electrical properties while maintaining the mechanical stability. Consequently, a small amount of graphene nanofillers are often added to the polymer matrix to form the graphene–polymer nanocomposites. In this way, superior electrical and mechanical properties compared to the matrix material can be attained with a low concentration of graphene loading [10,11].

To study the effective properties of graphene–polymer nanocomposites, a homogenization scheme is often required. Traditional homogenization analyses of graphene–polymer nanocomposites are primarily restricted to a single field such as pure electric field or pure thermal loading; multi-field coupled behaviors are rarely seen [12,13]. For instance, one may refer to Ji et al. [14] for a recent review. However, graphene–polymer nanocomposites are frequently subjected to the combination of thermal and electrical loadings in applications [15,16]. It turns out that temperature has a significant effect on the electrical properties of graphene and polymer, as well as on the interface characteristics between the graphene nanofillers and the polymer matrix [16]. There is a dire need to illustrate the influences of temperature and graphene volume concentration on the effective direct current (DC) electrical conductivity and dielectric permittivity of the nanocomposites. But at present, few micromechanics-based homogenization theories that can connect the temperature-dependent microstructural features to the temperature-dependent macroscopic behaviors seem to exist [17]. It is with this perspective that the present work was undertaken.

To develop a suitable homogenization scheme for the present problem, several issues need to be confronted. The first one is an appropriate homogenization scheme with a perfect interface [18]. This is a classic problem for two-phase composites. But common homogenization schemes are not sufficient for the electrical properties of graphene–polymer nanocomposites due to the strong interface effects and temperature-dependent properties of the constituent phases. In addition, graphene nanofillers are ultra-thin, so that the calculated effective properties may easily go outside the Hashin–Shtrikman (HS) bounds [12,19]. Percolation threshold is also a key issue in electrical conductivity. This is not a feature that every homogenization theory can address. To make sure that the predicted effective properties under a perfect interface will always lie on or within the HS bounds, and the percolation feature is self-contained in the theory, we will invoke the effective-medium approximation to serve as the backbone to start out the analysis.

The second issue is the temperature-dependent conductivity and permittivity of graphene fillers and polymer matrix, and the temperature-dependent interface effects between graphene fillers and polymer matrix. In the present setting, there are several interface effects. The first one is the imperfect mechanical bonding. A common way to address this issue is to include a weak interlayer around the graphene nanofillers; see, for instance, Nan et al. [20] and Duan et al. [21]. To study the temperature effect on the interlayer, we will introduce the concept of a temperature-degraded thermodynamics framework via the evolution of a degradation parameter. The thermodynamic driving force for the degradation process of the interlayer will be derived from the reduction of the degradation potential as the degradation proceeds. In addition, the corresponding thermodynamics-based evolution equation for the degradation parameter will be established based on the thermodynamics principle. It may be recognized that analogous processes have been previously invoked in the study of progressive damage of graphene–metal nanocomposites [22] and in the electric creep of ferroelectric ceramics [23]. In addition to the temperature degradation effect, there are two key interface factors that are unique in the electrical setting: the electron tunneling [24] and Maxwell–Wagner–Sillars (MWS) polarization [25–27]. These two factors are responsible for the extraordinarily high interfacial conductivity and dielectric permittivity, respectively, of the interface. While not commonly known, these two key factors are also temperature-dependent [28,29]. The underlying physics can be explained by the decreased electrons moving across the interface at higher temperature. Indeed, it is only after all these features are considered that one can arrive at a physically sound temperature-dependent homogenization scheme for the graphene–polymer nanocomposites.

In this work, we will present such a temperature-dependent homogenization theory to address the electrical conductivity and dielectric permittivity of graphene–polymer nanocomposites. The developed theory will be highlighted with a direct comparison to the experimental data of rGO/epoxy nanocomposites. Several novel features of the theory will be illustrated over a wide range of temperature and graphene concentration.

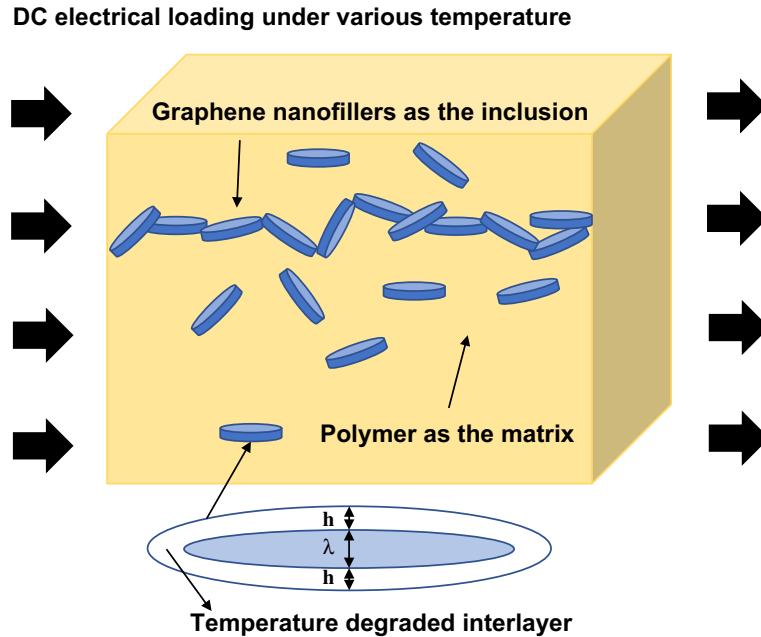


Fig. 1 Schematic of 3-D randomly distributed graphene–polymer nanocomposites subjected to DC electrical loading under various temperatures

The theoretical development will consist of three parts: (i) the temperature-dependent homogenization scheme for the electrical conductivity and dielectric permittivity of the nanocomposites; (ii) the temperature-dependent electrical properties of the constituent phases; and (iii) the temperature-dependent interface effects, including imperfect mechanical bonding represented by a temperature-degraded interlayer, the temperature-dependent electron tunneling across the interface, and the temperature-dependent MWS polarization at the interface.

We now turn to the development of the theory.

2 The temperature-dependent homogenization scheme for randomly distributed graphene–polymer nanocomposite

A typical morphology for the microstructure of graphene–polymer nanocomposites is depicted in Fig. 1. Graphene nanofillers are 3-D randomly distributed in the polymer matrix. The overall nanocomposite is subjected to DC electrical loading under certain temperature at infinity. The graphene phase in the specimen to be investigated later [7] is the graphene sheet with multilayer graphene patches instead of a single-layer graphene flake. It could be regarded as the highly oblate discoid with extremely low aspect ratio. Even though the graphene phase is very small and the accuracy of the micromechanical approach to the nanoscale problem can be a concern, some molecular dynamic simulations have rendered support that continuum modeling was adequately accurate for plates that are as thin as several atomic layers [30].

There are several homogenization schemes to achieve the effective properties of two-phase composites. The most common ways are the Ponte Castaneda–Willis (PCW) model [31], the Mori–Tanaka (MT) method [32] and the Bruggeman effective-medium approach (EMA) [33]. The PCW model can illustrate the percolation phenomenon of graphene nanocomposites, but the predicted outcomes will easily go out of the HS bound [19] even at low graphene loading. On the contrary, the calculated results via the MT method stay in the HS bounds, but it cannot depict the percolation phenomenon. Among these three, the EMA is the most suitable one for the present problem, as it possesses the percolation phenomenon and the calculated results always lie on or within the HS bounds [34].

The temperature-dependent effective-medium homogenization scheme of two-phase graphene–polymer nanocomposites can be evaluated from the zero-scattering of Maxwell’s far-field approach [18]

$$c_0 [(\mathbf{L}_0(T) - \mathbf{L}_e(T))^{-1} + \mathbf{S}_0 \mathbf{L}_e^{-1}(T)]^{-1} + c_1 \left\{ [(\mathbf{L}_1(T) - \mathbf{L}_e(T))^{-1} + \mathbf{S}_1 \mathbf{L}_e^{-1}(T)]^{-1} \right\} = \mathbf{0}, \quad (1)$$

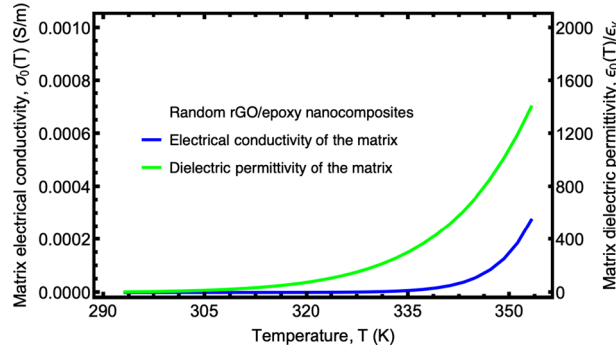


Fig. 2 The electrical conductivity and dielectric permittivity of the polymer matrix with respect to the temperature

where $\langle \cdot \rangle$ stands for the orientation average of the inside quantity. Parameters c_0 and c_1 represent the volume concentrations of the polymer matrix and graphene inclusion phases, respectively. Parameter T represents the absolute temperature in Kelvin, and \mathbf{S}_i is the temperature-independent Eshelby S-tensor of phase i , which is a strictly geometrical parameter [35]. Tensor $\mathbf{L}_i(T)$ denotes the temperature-dependent homogenization parameter of phase i , which can be electrical conductivity or dielectric permittivity, thermal conductivity, elastic modulus, etc. Subscripts of “0”, “1” and “e” stand for the properties of matrix phase, inclusion phase and effective medium, in turn. In the present paper, electrical conductivity and dielectric permittivity are adopted as the homogenization parameters.

As the graphene inclusions are transversely isotropic with direction 3 being symmetric, the orientational averages in Eq. (1) give rise to the corresponding scalar equations for the isotropic effective electrical conductivity, σ_e , and dielectric permittivity, ε_e , of overall nanocomposites, respectively, as

$$c_0 \frac{\sigma_0(T) - \sigma_e(T)}{\sigma_e(T) + (1/3)(\sigma_0(T) - \sigma_e(T))} + \frac{1}{3} c_1 \left[\frac{2(\sigma_1(T) - \sigma_e(T))}{\sigma_e(T) + S_{11}(\sigma_1(T) - \sigma_e(T))} + \frac{\sigma_3(T) - \sigma_e(T)}{\sigma_e(T) + S_{33}(\sigma_3(T) - \sigma_e(T))} \right] = 0, \quad (2)$$

$$c_0 \frac{\varepsilon_0(T) - \varepsilon_e(T)}{\varepsilon_e(T) + (1/3)(\varepsilon_0(T) - \varepsilon_e(T))} + \frac{1}{3} c_1 \left[\frac{2(\varepsilon_1(T) - \varepsilon_e(T))}{\varepsilon_e(T) + S_{11}(\varepsilon_1(T) - \varepsilon_e(T))} + \frac{\varepsilon_3(T) - \varepsilon_e(T)}{\varepsilon_e(T) + S_{33}(\varepsilon_3(T) - \varepsilon_e(T))} \right] = 0, \quad (3)$$

where $\sigma_0(T)$, $\sigma_1(T)$, $\sigma_3(T)$, $\varepsilon_0(T)$, $\varepsilon_1(T)$, $\varepsilon_3(T)$ are the temperature-dependent conductivity and permittivity of the polymer matrix and graphene inclusion phases, which will be given in Sect. 3. If the inclusion phase is regarded as a discoid, the components of the Eshelby S-tensor of graphene nanofiller phase, \mathbf{S}_1 , are given by [35]

$$\begin{aligned} S_{11} = S_{22} &= \frac{\alpha}{2(1 - \alpha^2)^{3/2}} \left[\arccos \alpha - \alpha(1 - \alpha^2)^{1/2} \right], \\ S_{33} &= 1 - 2S_{11}, \end{aligned} \quad (4)$$

where $\alpha (< 1)$ stands for the graphene aspect ratio (the thickness-to-diameter ratio). In addition, the Eshelby S-tensor of the matrix phase, \mathbf{S}_0 , can degenerate to $S_{11}^0 = S_{33}^0 = 1/3$ when regarded as a sphere.

3 The temperature-dependent electrical properties for the constituent phases

The electrical properties of the constituent phases cannot remain constant when subjected to varying temperature. In this section, we will explore the influences of temperature on the electrical properties for the graphene nanofiller and polymer matrix phases, respectively.

3.1 Temperature-dependent electrical conductivity and dielectric permittivity for the polymer matrix phase

Polymer is an insulator. Its electrical conductivity and dielectric permittivity are intrinsically dependent on temperature like most insulators. As temperature increases, some electrons acquire energy and then become free for electrical conduction. Hence, the electrical conductivity of polymer matrix increases with temperature. On the other hand, the dielectric permittivity depends on the polarization of molecules by the electric field.

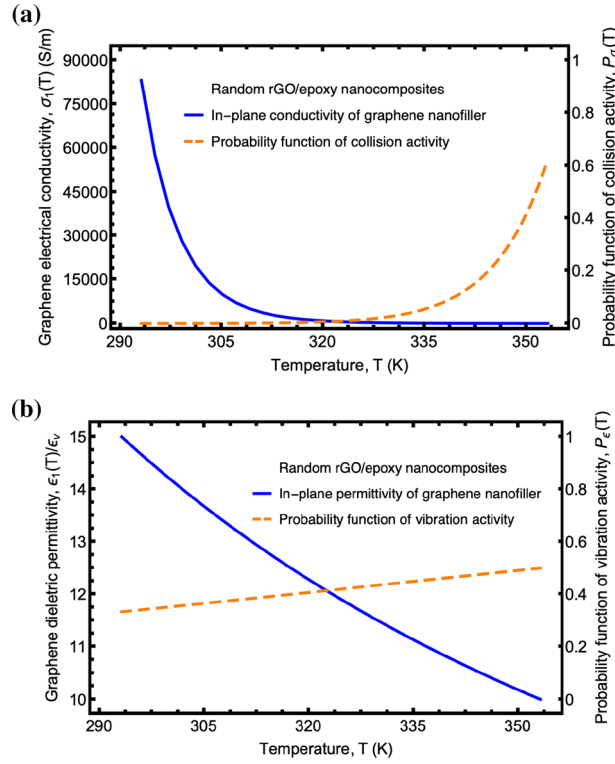


Fig. 3 **a** The in-plane electrical conductivity of graphene nanofiller and probability function of collision activity with respect to the temperature. **b** The in-plane dielectric permittivity of graphene nanofiller and probability function of vibration activity with respect to the temperature

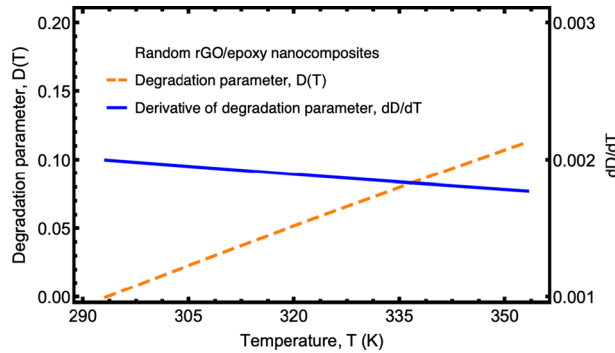


Fig. 4 The degradation parameter and its derivative for the interlayer between the graphene nanofiller and polymer matrix with respect to the temperature

As more electrons become free at higher temperature, more molecules can be more easily polarized by an electric field. Therefore, the dielectric permittivity of polymer matrix also increases with temperature. This temperature-dependent trend of polymer permittivity agrees with the predictions by Švorčík et al. [36] and Hyun et al. [37].

With this perspective, the influence of temperature on the conductivity and permittivity can be described via the Arrhenius equation as [29,38]

$$\sigma_0(T) = \xi_0^\sigma e^{-E_0^\sigma/k_B T}, \tag{5}$$

$$\epsilon_0(T) = \xi_0^\epsilon e^{-E_0^\epsilon/k_B T}, \tag{6}$$

where $k_B = 1.38 \times 10^{-23} \text{ m}^2 \text{ kg/s}^2 \text{ K}$ is the Boltzmann constant, E_0^σ and E_0^ϵ are the activation energies for the electrical conductivity and dielectric permittivity of polymer matrix, respectively, and ξ_0^σ and ξ_0^ϵ are

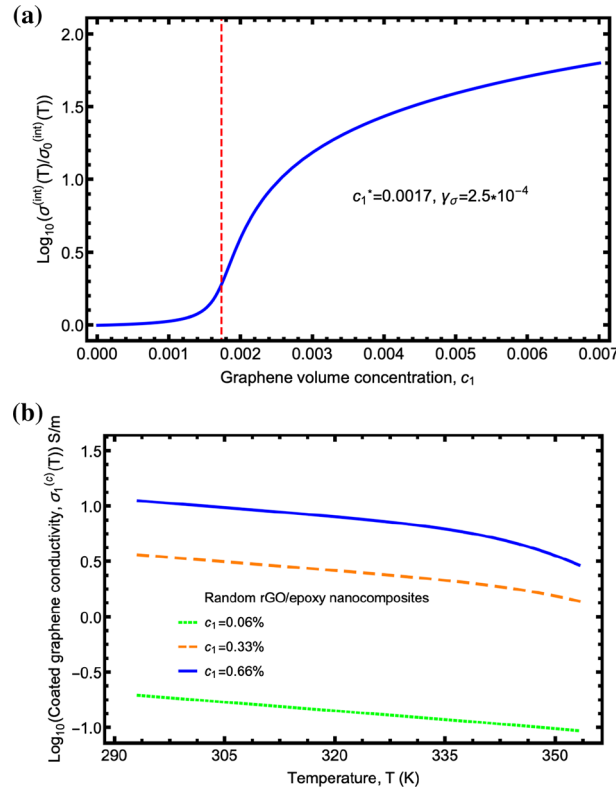


Fig. 5 **a** The electrical conductivity of the interlayer with respect to the graphene volume concentration. **b** The in-plane electrical conductivity of coated graphene nanofillers with respect to the temperature

the corresponding prefactors. The electrical conductivity and dielectric permittivity of polymer matrix both increase with temperature, as shown in Fig. 2.

3.2 Temperature-dependent electrical conductivity and dielectric permittivity for the graphene nanofiller phase

Graphene is a highly conducting medium. Its electrical conductivity and dielectric permittivity also depend on temperature like most conductors [39]. At low temperature, the energy of carbon ions remains at a low level, but as temperature increases, its ions will acquire more energy and start to oscillate about their mean positions. The oscillating ions tend to collide more easily with the moving electrons and reduce the conductivity. Thus, the electrical conductivity will decrease with temperature due to the increased collision activity between free electrons and carbon ions. For its permittivity, it is observed that as temperature increases, the vibrating state of carbon ions will increase. The carbon ions at high temperature do not easily point to the direction of the electric field as at low temperature. As a result, its dielectric permittivity will decrease with temperature due to the increased level of vibration activity of carbon ions.

With this view, the temperature-dependent in-plane conductivity and permittivity of graphene nanofillers can be written to be inversely dependent on the collision and vibration activities, respectively, as

$$\sigma_1(T) = \sigma_1^{(0)} / P_\sigma(T), \quad (7)$$

$$\varepsilon_1(T) = \varepsilon_1^{(0)} / P_\varepsilon(T), \quad (8)$$

where $\sigma_1^{(0)}$ and $\varepsilon_1^{(0)}$ are the in-plane electrical conductivity and dielectric permittivity of graphene nanofiller at $P_\sigma(T) = 1$ and $P_\varepsilon(T) = 1$, respectively. By taking the collision and vibration activities as temperature-controlled statistical processes, the functions $P_\sigma(T)$ and $P_\varepsilon(T)$ can be modeled by the Arrhenius equation [29,38] as

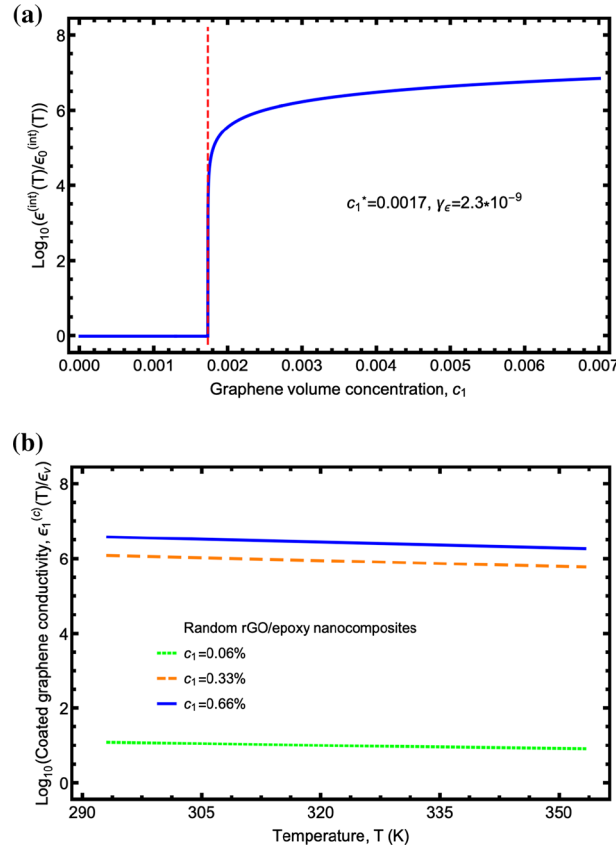


Fig. 6 **a** The dielectric permittivity of the interlayer with respect to the graphene volume concentration. **b** The in-plane dielectric permittivity of coated graphene nanofiller with respect to the temperature

$$P_{\sigma}(T) = \xi_1^{\sigma} e^{-E_1^{\sigma}/k_B T}, \quad (9)$$

$$P_{\varepsilon}(T) = \xi_1^{\varepsilon} e^{-E_1^{\varepsilon}/k_B T}, \quad (10)$$

where E_1^{σ} and E_1^{ε} are the activation energies for the collision and vibration process of carbon ions, respectively, and ξ_1^{σ} and ξ_1^{ε} are prefactors. To describe the transverse isotropy of graphene, its out-of-plane properties can be written as

$$\sigma_3(T) = m\sigma_1(T), \quad \varepsilon_3(T) = n\varepsilon_1(T), \quad (11)$$

with $m = 10^{-3}$ and $n = 0.67$ commonly adopted.

To provide some insights, the in-plane electrical conductivity of graphene nanofillers and probability of collision process are shown in Fig. 3a. The graphene conductivity decreases with temperature, while the collision probability increases with it. This description agrees with the trends reported by Bolotin et al. [39] and Huang et al. [40]. Figure 3b depicts the in-plane dielectric permittivity and probability of vibration process of graphene nanofillers with respect to temperature. This prediction of temperature-dependent graphene permittivity also agrees with the trend reported by Huang et al. [40].

4 The temperature-dependent interface effects between the constituent phases

The effective electrical properties of overall nanocomposites given in Eqs. (2) and (3) are only for the perfect interface condition. However, the interface condition between the constituent phases cannot be perfect in practical applications. The interface between the graphene phase and the polymer phase is considered as an ultra-thin isotropic interlayer surrounding the graphene nanofiller. The schematic of imperfect interlayer is depicted in the inset of Fig. 1. Three categories of temperature-dependent interface effects are included for the interface. The first one is the temperature-dependent imperfect mechanical bonding effect with degraded

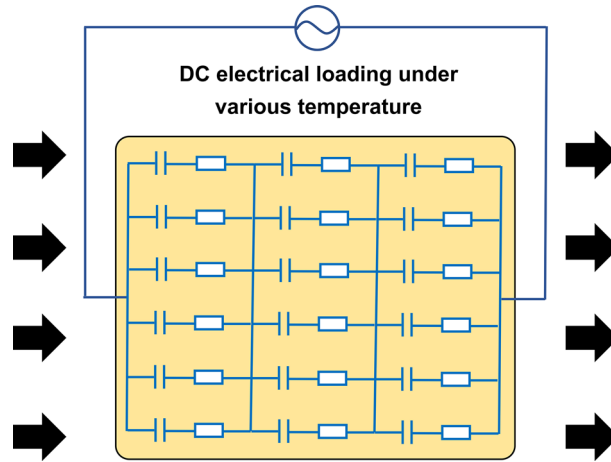


Fig. 7 Schematics of the temperature-dependent Maxwell–Wagner–Sillars polarization effect between the constituent phases

interlayer. The second one is the temperature-dependent electron tunneling effect across the interface, and the third one is the temperature-dependent MWS polarization at the interface. Consideration of all of them is essential for the temperature-dependent homogenization scheme of graphene–polymer nanocomposites.

4.1 Temperature-dependent imperfect interfacial bonding effect with degraded process

As a first step, the temperature-dependent imperfect mechanical bonding effect will be considered between the graphene and polymer phases. It tends to lower the effective properties of the overall nanocomposites [13]. A temperature-degraded interlayer with lower electrical properties will be introduced around the graphene inclusion to form the coated graphene nanofillers. The graphene nanofiller is fully surrounded by an isotropic interlayer with a constant thickness. The Mori–Tanaka method [32] is the most suitable approach for the present fully surrounded case. It is convenient to evaluate the electrical conductivity and dielectric permittivity of the coated nanofiller as

$$\sigma_i^{(c)}(T) = \sigma_0^{(\text{int})}(T) \left[1 + \frac{(1 - c_{\text{int}})(\sigma_i - \sigma_0^{(\text{int})}(T))}{c_{\text{int}} S_{ii}(\sigma_i - \sigma_0^{(\text{int})}(T)) + \sigma_0^{(\text{int})}(T)} \right], \quad (12)$$

$$\varepsilon_i^{(c)}(T) = \varepsilon_0^{(\text{int})}(T) \left[1 + \frac{(1 - c_{\text{int}})(\varepsilon_i - \varepsilon_0^{(\text{int})}(T))}{c_{\text{int}} S_{ii}(\varepsilon_i - \varepsilon_0^{(\text{int})}(T)) + \varepsilon_0^{(\text{int})}(T)} \right], \quad (13)$$

where S_{ii} is the ii -component of the Eshelby S-tensor for the graphene nanofiller, S_1 . $\sigma_0^{(\text{int})}(T)$ and $\varepsilon_0^{(\text{int})}(T)$ are the temperature-dependent isotropic conductivity and permittivity of the degraded interlayer, respectively. c_{int} is the volume concentration of the interlayer in the coated nanofiller configuration [13]

$$c_{\text{int}} = 1 - \frac{\lambda}{2} \left(\frac{\lambda}{2\alpha} \right)^2 / \left(\frac{\lambda}{2} + h \right) \left(\frac{\lambda}{2\alpha} + h \right)^2 \approx 2(1 + 2\alpha) \frac{h}{\lambda}. \quad (14)$$

where h and λ are the thickness of the interlayer and graphene nanofiller, respectively.

In order to depict the degradation of the interfacial electrical properties with respect to the temperature, a degradation parameter, $D(T)$, is introduced to connect the properties of the interlayer in the degraded and perfect states

$$\sigma_0^{(\text{int})}(T) = \sigma_r^{(\text{int})} [1 - D(T)], \quad (15)$$

$$\varepsilon_0^{(\text{int})}(T) = \varepsilon_r^{(\text{int})} [1 - D(T)], \quad (16)$$

where as in the terminology of damage mechanics, $D = 0$ and $D = 1$ represent the perfect state and fully degraded state, respectively. $\sigma_r^{(\text{int})}$ and $\varepsilon_r^{(\text{int})}$ are the interfacial conductivity and permittivity at the perfect, reference state ($D = 0$).

Table 1 The geometrical parameters and physical properties used in the numerical simulation of the temperature-dependent electrical conductivity and dielectric permittivity of randomly distributed rGO/epoxy nanocomposites for validation with Yousefi et al. [7]

Parameters and physical properties used in the numerical simulation	Values
Aspect ratio of the graphene nanofiller, α	9.8×10^{-4}
Thickness of graphene nanofiller, λ (m)	5×10^{-8}
Thickness of the interlayer, h (m)	6×10^{-9}
Electrical conductivity of the interlayer at $c_1 = 0$, $\sigma_r^{(int)}$ (S/m)	3.55×10^{-5}
Relative dielectric permittivity of the interlayer at $c_1 = 0$, $\varepsilon_r^{(int)}/\varepsilon_v$	3
Scale parameter of the electronic tunneling effect at the interface, γ_σ	2.5×10^{-4}
Scale parameter of the MWS effect at the DC state, γ_ε	2.3×10^{-9}
Dielectric permittivity in the vacuum, ε_v (F/m)	8.85×10^{-12}
Parameter in the evolution equation, $a_1 L$	2×10^{-3}
Prefactor for conductivity of polymer matrix, ξ_0^σ (S/m)	3.69×10^{25}
Prefactor for permittivity of polymer matrix, $\xi_0^\varepsilon/\varepsilon_v$	2.24×10^{15}
Prefactor for conductivity of graphene nanofillers, $\sigma_1^{(0)}/\xi_1^\sigma$ (S/m)	1.89×10^{-19}
Prefactor for permittivity of graphene nanofillers, $\varepsilon_1^{(0)}/\varepsilon_v \xi_1^\varepsilon$	1.38
Initial temperature for interfacial temperature degradation process, T_0 (K)	293.15
Activation energy for conductivity of polymer matrix, E_0^σ (J)	3.27×10^{-19}
Activation energy for permittivity of polymer matrix, E_0^ε (J)	1.37×10^{-19}
Activation energy for conductivity of graphene nanofiller, E_1^σ (J)	2.20×10^{-19}
Activation energy for permittivity of graphene nanofiller, E_1^ε (J)	9.65×10^{-21}

As temperature rises, the interlayer will degrade. This is an irreversible dissipation process. The principle of non-equilibrium thermodynamics leads to

$$-\frac{\partial \psi_D}{\partial D} dD \geq 0, \quad (17)$$

where the thermodynamics-based degradation potential, ψ_D , can be expressed by a single-well function

$$\psi_D = a_1 D(T) [D(T) - 2] + a_0, \quad (18)$$

in which a_0 and a_1 are degradation constants. The corresponding thermodynamic driving force for the temperature-degraded process of the interlayer can be derived by the negative derivative of degradation potential with respect to D [41]

$$f_{\text{driv}} = -\frac{\partial \psi_D}{\partial D} = 2a_1 [1 - D(T)]. \quad (19)$$

Note that the thermodynamic driving force is conjugate to the growth of degradation parameter.

Then, it is necessary to derive the evolution equation for the degradation parameter as a function of the thermodynamic driving force [22]

$$\frac{dD}{dT} = \begin{cases} L \cdot f_{\text{driv}}, & T \geq T_0 \\ 0, & T < T_0 \end{cases}, \quad \text{with } D(T \leq T_0) = 0, \quad (20)$$

where the derivative of the degradation parameter with respect to the temperature is taken to be proportional to the thermodynamic driving force. Here L is a constant parameter of the evolution equation, and T_0 is the initial temperature for degradation process of the interlayer. With this kinetic equation, the degradation parameter will increase with the temperature from 0 to 1. The corresponding solution of the degradation parameter, $D(T)$, is

$$D(T) = 1 - e^{-2a_1 L(T-T_0)}, \quad \text{with } D(T \leq T_0) = 0. \quad (21)$$

Note that the relationship between dD and dT in Eq. (20) is similar to the time-dependent Ginzburg–Landau (TDGL) kinetic equation for the order parameter [42,43], which has been widely used in the phase-field simulation of the microstructural features of ferroelectric nanofilms [44]. Similar evolution equations have been adopted in the degradation process of graphene–metal nanocomposites [22] and the domain evolution of ferroelectric ceramics [23]. The variations of the degradation parameter and its derivative with respect to the temperature are given in Fig. 4. The degradation parameter increases with the temperature, while its derivative decreases with respect to it.

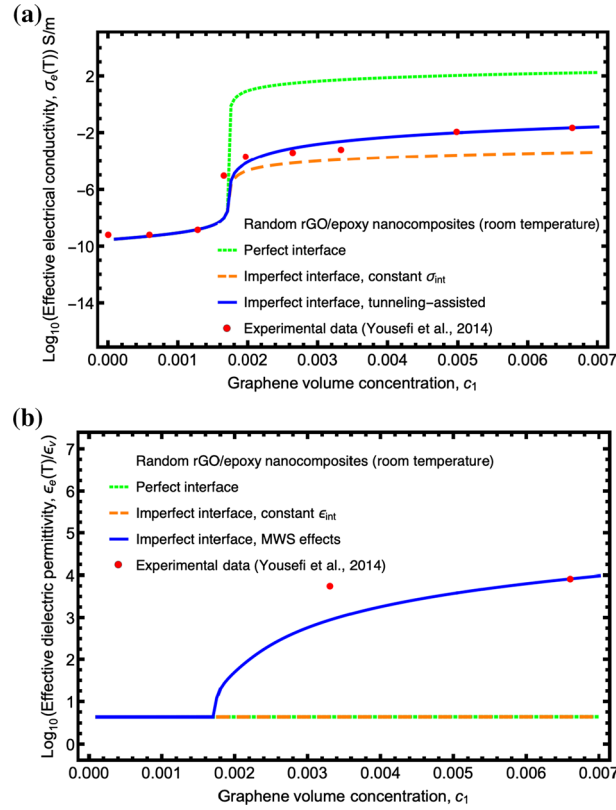


Fig. 8 The effective **a** electrical conductivity and **b** dielectric permittivity of graphene–polymer nanocomposites with respect to the graphene volume concentration under different interface conditions at the room temperature

4.2 The temperature-dependent electron tunneling effect for interfacial conductivity

Next, we consider the temperature-dependent electron tunneling effect between the graphene nanofiller and polymer matrix. To model the interfacial tunneling effect across the interface, the temperature-dependent interfacial conductivity with this additional effect can be expressed as

$$\sigma_{\text{tunneling}}^{(\text{int})}(T) = \sigma_0^{(\text{int})}(T) / \tau(c_1, c_1^*, \gamma_\sigma), \quad (22)$$

where as in the representation of electron tunneling in CNT- and graphene–polymer nanocomposites, $F(c_1, c_1^*, \gamma_\sigma)$ is Cauchy's cumulative probabilistic function [45], defined by

$$F(c_1, c_1^*, \gamma_\sigma) = \frac{1}{\pi} \arctan\left(\frac{c_1 - c_1^*}{\gamma_\sigma}\right) + \frac{1}{2}, \quad \text{with } \tau(c_1, c_1^*, \gamma_\sigma) = \frac{F(1, c_1^*, \gamma_\sigma) - F(c_1, c_1^*, \gamma_\sigma)}{F(1, c_1^*, \gamma_\sigma) - F(0, c_1^*, \gamma_\sigma)}. \quad (23)$$

In this function, γ_σ is the scaling parameter for the electron tunneling effect, and c_1^* is the percolation threshold for the two-phase nanocomposite [13]

$$c_1^* = \frac{9S_{33}(1 - S_{33})}{-9S_{33}^2 + 15S_{33} + 2}. \quad (24)$$

The electron tunneling effect improves interfacial conductivity remarkably after the percolation threshold, as depicted in Fig. 5a. The underlying reason can be illustrated that the average distance between the adjacent nanofillers decreases as graphene loading passes through the percolation threshold. At this stage the graphene connective networks build up rapidly. As a result, it significantly improves the probability of electron tunneling phenomenon.

While filler loading can improve the interfacial conductivity, the temperature level will also have an effect on the electron tunneling. Due to the increased collision activity of electrons at higher temperature, the

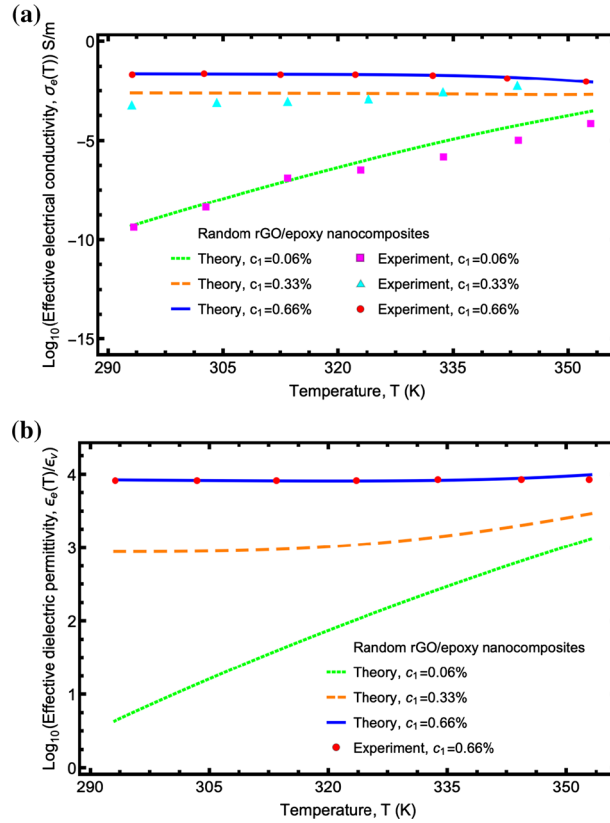


Fig. 9 The effective **a** electrical conductivity and **b** dielectric permittivity of graphene–polymer nanocomposites with respect to the temperature at various graphene nanofiller loadings

interfacial conductivity tends to decrease with it, as explained for Eq. (7). As a consequence, the effective conductivity of the “coated” graphene nanofiller, $\sigma_i^{(c)}(T)$, is obtained by replacing the $\sigma_0^{(int)}(T)$ in Eq. (12) with this $\sigma_{\text{tunneling}}^{(int)}(T)$. Figure 5b shows the decreasing in-plane conductivity of the coated graphene nanofiller with temperature due to the combined effects of this temperature-dependent electron tunneling and the earlier temperature degradation of the interlayer at three levels of graphene loadings.

4.3 The temperature-dependent Maxwell–Wagner–Sillars polarization effect for interfacial permittivity

Thirdly, we explore the temperature-dependent MWS polarization effect at the interface. The temperature-dependent interfacial permittivity with the additional MWS effect can be expressed as

$$\epsilon_{\text{MWS}}^{(int)}(T) = \epsilon_0^{(int)}(T)/\tau(c_1, c_1^*, \gamma_\epsilon), \quad (25)$$

where γ_ϵ is the scaling parameter for the MWS polarization effect. The MWS polarization effect enhances the interfacial permittivity significantly after the percolation threshold, as depicted in Fig. 6a. The underlying physics is that due to the huge disparity of electrical conductivity of graphene and polymer phases, electrons cannot freely flow across the interlayer between the graphene nanofiller and polymer matrix. This leads to the formation of numerous nanocapacitors at the interface. Each nanocapacitor can be physically modeled by a series connection of a capacitor and a resistor, as depicted in Fig. 7. This phenomenon is described by the τ -function in Eq. (25).

In addition, the temperature also has influences on the MWS polarization effect. Replacing the $\epsilon_0^{(int)}(T)$ in Eq. (13) with this $\epsilon_{\text{MWS}}^{(int)}(T)$, we will obtain the effective permittivity for the “coated” graphene nanofiller, $\epsilon_i^{(c)}$, at a given level of c_1 and T . Figure 6b shows the decreasing in-plane permittivity of the coated graphene nanofiller

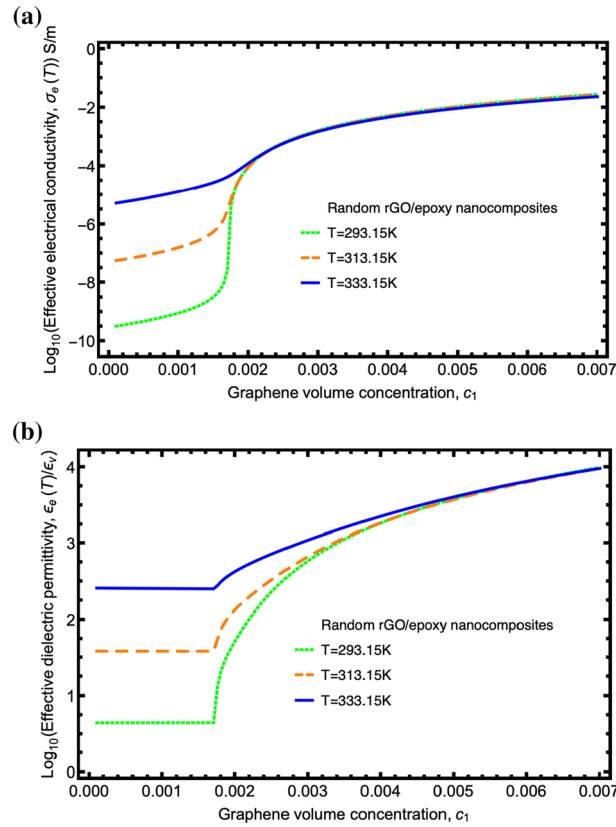


Fig. 10 The effective **a** electrical conductivity and **b** dielectric permittivity of graphene–polymer nanocomposites with respect to the graphene volume concentration under various temperatures

with temperature due to the combination of the temperature-dependent MWS effect and the degradation of the interlayer at three levels of graphene loading.

At this stage, the temperature-dependent homogenization theory is completely developed. The temperature-dependent “coated” $\sigma_i^{(c)}(T)$ and $\epsilon_i^{(c)}(T)$ in Eqs. (12) and (13) can now be used to replace the original $\sigma_i(T)$ and $\epsilon_i(T)$ of the inclusion phase in Eqs. (2) and (3), to calculate the temperature-dependent effective conductivity and permittivity, $\sigma_e(T)$ and $\epsilon_e(T)$, of the overall nanocomposite.

5 Results and discussion

To place the present temperature-dependent homogenization theory in proper perspective, a direct comparison will be made to the experimental data for the effective conductivity and permittivity of rGO/epoxy nanocomposite over a wide range of temperature [7]. As their data were given in the weight percentage (wt%) of graphene nanofillers, it needs to be changed to the volume percentage (vol%) for the theoretical prediction. The relationship between the two quantities is

$$\text{vol}\% = \rho_m / \left[\rho_m + \rho_g \left(\frac{1}{\text{wt}\%} - 1 \right) \right], \quad (26)$$

where $\rho_m = 1250 \text{ kg/m}^3$ and $\rho_g = 1900 \text{ kg/m}^3$ are the mass densities of the epoxy polymer and graphene nanofiller, respectively [46]. In addition, the geometrical parameters and material properties utilized in the numerical simulation are given in Table 1 according to the experimental conditions.

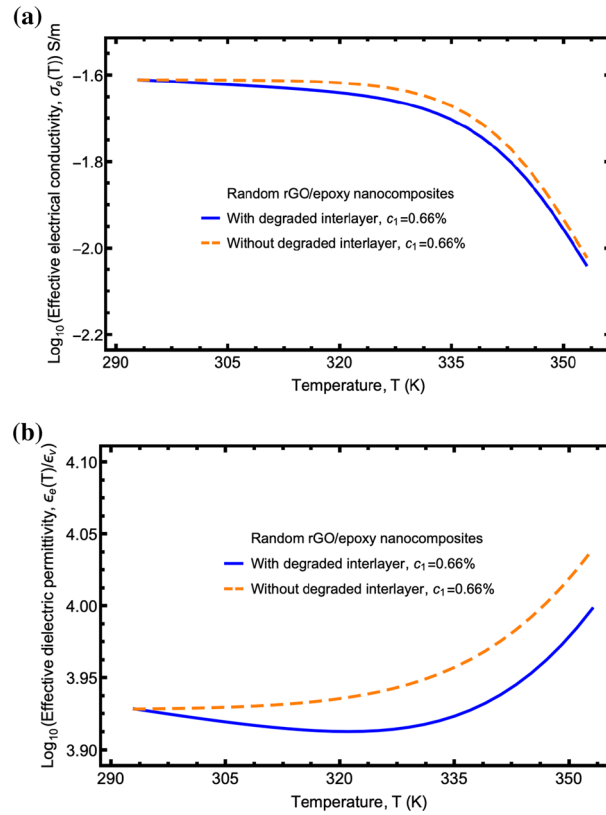


Fig. 11 The influences of the degraded interlayer for the effective **a** electrical conductivity and **b** dielectric permittivity of graphene–polymer nanocomposites

5.1 Validation of the present temperature-dependent homogenization model at room temperature

First, the present homogenization model for the electrical properties is validated at a certain room temperature. Three categories of interface conditions are considered during numerical simulations: (i) the perfect interface condition; (ii) the imperfect interface condition with constant interfacial conductivity and permittivity; and (iii) the imperfect interface condition with electron tunneling and MWS polarization effects.

To begin with, the effective conductivity is obtained under the perfect interface condition, as revealed in the green line of Fig. 8a. The calculated conductivity is seen to be much higher than the experimental data, which implies the existence of imperfect interface effects. After considering the imperfect mechanical bonding effect with constant interfacial conductivity, the effective conductivity is found to decrease as shown by the yellow line of Fig. 8a. But the numerical result is lower than the experimental data. After considering the interfacial tunneling effect, the theoretical prediction agrees with the experimental data [7], as depicted by the blue line of Fig. 8a. Similar numerical simulations are obtained for effective permittivity at a certain temperature. The calculated permittivity is much lower than the experimental data under the perfect interface condition or the imperfect mechanical bonding effect with constant interfacial permittivity, as shown by the overlapping green and yellow lines of Fig. 8b. After considering the MWS polarization effect, the numerical result improves significantly after the percolation threshold and agrees with the experimental data [7], as depicted by the blue line of Fig. 8b. It is demonstrated that the present homogenization model is validated for effective conductivity and permittivity.

5.2 Influences on effective electrical properties at various temperatures

Then, we explore the effective electrical conductivity and dielectric permittivity of the nanocomposites with respect to temperature. All three categories of temperature-dependent interface effects are considered during the numerical simulations. Three graphene loadings are investigated in this subsection: $c_1 = 0.06\%$, $c_1 = 0.33\%$

and $c_1 = 0.66\%$. The first one is the case before the percolation threshold, while the last two correspond to the cases after that.

Figure 9a depicts the effective electrical conductivity of the nanocomposites with respect to temperature at the same three graphene concentrations. The effective electrical conductivity increases with temperature before the percolation threshold (the bottom line), but the influence of temperature declines significantly after that (the top two lines). The effective conductivity continues to decrease slightly with temperature after the percolation threshold. On the other hand, Fig. 9b shows the effective dielectric permittivity of the nanocomposites with respect to temperature at the same three graphene volume concentrations. The effective dielectric permittivity also increases with respect to the temperature before the percolation threshold. After that, it increases slightly with temperature, which is opposite to the trend of effective conductivity. These predictions of conductivity and permittivity with respect to temperature are consistent with the experimental data of Yousefi et al. [7]. This trend also agrees with the experiment of Cao et al. [38].

5.3 Influences on effective electrical properties at various graphene concentrations

Next, we investigate effective electrical properties of the nanocomposites with respect to graphene concentrations at various temperatures. The effective electrical conductivity and dielectric permittivity increase with respect to the graphene nanofiller loading, as depicted in Figs. 10a, b. Note that the differences among these cases under different temperature are significant before the percolation threshold. However, the influence of temperature on the effective properties tends to decrease after the percolation threshold. It is concluded that the temperature has more significant effect at low graphene loadings.

5.4 Influences of temperature-degraded interlayer on effective electrical properties

Finally, we investigate the influences of temperature-degraded interlayer on the effective electrical properties of the nanocomposites. Figures 11a, b illustrate the calculated conductivity and permittivity with and without the temperature-degraded interlayer. It is evident that the calculated effective properties will have a different characteristic if the overall behavior of the nanocomposites is evaluated without considering the temperature-degraded interlayer. The effective conductivity and permittivity with degraded interlayer are clearly lower than those without considering it. The separation points of these two cases are the onset of the temperature-dependent degradation process of the interlayer at $T = T_0$.

6 Concluding remarks

In this work we have developed a temperature-dependent homogenization theory for the electrical conductivity and dielectric permittivity of graphene–polymer nanocomposites. We first invoked a temperature-dependent effective-medium theory homogenization scheme with a perfect interface. Then, the temperature-dependent constitutive equations for the electrical conductivity and dielectric permittivity of polymer and graphene were introduced. In this process, we have considered the activation of free electrons and polarization of molecules for the polymer phase, and the collision and vibration probabilities for graphene. Finally, the temperature-dependent interface effects between graphene fillers and polymer matrix were investigated. These include the temperature-dependent imperfect mechanical bonding, the temperature-dependent electron tunneling, as well as the temperature-dependent MWS polarization effects. These interfacial and constituent properties were then integrated into the original effective-medium framework to build the complete theory.

After the theory is developed, we have validated it with rGO/epoxy nanocomposites over the temperature range from 293 to 353 K. It is demonstrated that the effective electrical conductivity and dielectric permittivity increase with respect to the temperature before the percolation threshold. But after the percolation threshold, the influences of temperature on effective electrical properties are shown to decrease significantly. The effective dielectric permittivity continues to increase slightly with temperature, while an opposite trend is revealed for effective electrical conductivity. In addition, the influence of temperature on effective electrical properties is markedly higher at low graphene loading.

We conclude by saying that temperature-dependent phenomenon of electrical properties did not only occur in graphene–polymer nanocomposite, but also in CNT–polymer [47] and carbon-fiber composites [38]. At present, the study of temperature-dependent electrical properties mainly focuses on the glassy state of the

polymer phase; it does not involve the temperature range involving the glass transition temperature, T_g . Epoxy is a thermoset; its glass transition temperature is not sharp. To study the T_g -involved properties, the change of electrical conductivity and dielectric permittivity of epoxy on both sides of T_g has to be determined first. The dependence of T_g of the composite on graphene volume concentration also has to be specified. Some MD simulations have indicated that T_g of graphene–epoxy composites is higher than that of pure epoxy, but the nature of change also depends on the functionalization of graphene [48]. This is an important but complex problem. In this work, we only consider the temperature range without involving the gradual transition of amorphous materials. Within this range, there are sufficient applications for graphene nanocomposites. The presented temperature-dependent homogenization theory has taken into account many intrinsic features of the underlying physical processes. These include the temperature-dependent constitutive equations of polymers and graphene, the temperature-degraded interlayer, and the temperature-dependent electron tunneling and Maxwell–Wagner–Sillars polarization. The theory is capable of providing the effective conductivity and dielectric permittivity of the graphene–polymer nanocomposites in a quantitative way. The theoretical predictions have been validated with the experimental data over a wide range of temperature and graphene concentrations. It is believed that this theory can be readily applied to guide the design and applications of graphene–polymer nanocomposites.

Acknowledgements Xiaodong Xia thanks the support of National Natural Science Foundation of China (Grant Nos. 11902365), the ‘Future Talents’ short-term scholarship from TU Darmstadt, and the initial funding from Central South University (Grant Nos. 202045014). George J. Weng thanks the support of NSF Mechanics of Materials and Structures Program under CMMI-1162431. Juanjuan Zhang thanks the support of National Natural Science Foundation of China (Grant No. 11702120). Yang Li thanks the support of the Natural Science Foundation of Hunan Province (Grant No. 2019JJ50768), and initial funding from Central South University (Grant No. 202045006).

References

1. Fan, S., Feng, X., Han, Y., Fan, Z., Lu, Y.: Nanomechanics of low-dimensional materials for functional applications. *Nanoscale Horiz.* **4**, 781–788 (2019)
2. Ji, L., Meduri, P., Agubra, V., Xiao, X., Alcoutlabi, M.: Graphene-based nanocomposites for energy storage. *Adv. Energy Mater.* **6**, 1502159 (2016)
3. Faroughi, S., Rojas, E., Abdelkefi, A., Park, Y.: Reduced-order modeling and usefulness of non-uniform beams for flexo-electric energy harvesting applications. *Acta Mech.* **230**, 2339–2361 (2019)
4. Hossain, M., Li, J.: Frequency-dependent dielectric properties of BTO/parylene nanocomposites with layered structure. *Acta Mech.* **229**, 929–937 (2018)
5. Eswaraiah, V., Balasubramaniam, K., Ramaprabhu, S.: Functionalized graphene reinforced thermoplastic nanocomposites as strain sensors in structural health monitoring. *J. Mater. Chem.* **21**, 12626–12628 (2011)
6. Moriche, R., Jiménez-Suárez, A., Sánchez, M., Prolongo, S.G., Ureña, A.: High sensitive damage sensors based on the use of functionalized graphene nanoplatelets coated fabrics as reinforcement in multiscale composite materials. *Compos. Part B Eng.* **149**, 31–37 (2018)
7. Yousefi, N., Sun, X., Lin, X., Shen, X., Jia, J., Zhang, B., et al.: Highly aligned graphene/polymer nanocomposites with excellent dielectric properties for high-performance electromagnetic interference shielding. *Adv. Mater.* **26**, 5480–5487 (2014)
8. Chen, Y., Zhang, H.B., Yang, Y.B., Wang, M., Cao, A.Y., Yu, Z.Z.: High-performance epoxy nanocomposites reinforced with three-dimensional carbon nanotube sponge for electromagnetic interference shielding. *Adv. Funct. Mater.* **26**, 447–455 (2016)
9. Geim, A.K., Novoselov, K.S.: The rise of graphene. *Nat. Mater.* **6**, 183–191 (2007)
10. Zhou, X., Li, D., Wan, S., Cheng, Q., Ji, B.: In silicon testing of the mechanical properties of graphene oxide-silk nanocomposites. *Acta Mech.* **230**, 1413–1425 (2019)
11. Cong, P.H., Duc, N.D.: New approach to investigate the nonlinear dynamic response and vibration of a functionally graded multilayer graphene nanocomposite plate on a viscoelastic Pasternak medium in a thermal environment. *Acta Mech.* **229**, 3651–3670 (2018)
12. Pan, Y., Weng, G.J., Meguid, S.A., Bao, W.S., Zhu, Z., Hamouda, A.: Percolation threshold and electrical conductivity of a two-phase composite containing randomly oriented ellipsoidal inclusions. *J. Appl. Phys.* **110**, 123715 (2011)
13. Wang, Y., Shan, J.W., Weng, G.J.: Percolation threshold and electrical conductivity of graphene-based nanocomposites with filler agglomeration and interfacial tunneling. *J. Appl. Phys.* **118**, 065101 (2015)
14. Ji, X., Xu, Y., Zhang, W., Cui, L., Liu, J.: Review of functionalization, structure and properties of graphene/polymer composite fibers. *Compos. Part A* **87**, 29–45 (2016)
15. Wang, X., Gong, L.X., Tang, L.C., Peng, K., Pei, Y.B., Zhao, L., et al.: Temperature dependence of creep and recovery behaviors of polymer composites filled with chemically reduced graphene oxide. *Compos. Part A* **69**, 288–298 (2015)
16. Cao, W.Q., Wang, X.X., Yuan, J., Wang, W.Z., Cao, M.S.: Temperature dependent microwave absorption of ultrathin graphene composites. *J. Mater. Chem. C* **3**, 10017–10022 (2015)
17. Zhou, T., Boyd, J.G., Lutkenhaus, J.L., Lagoudas, D.C.: Micromechanics modeling of the elastic moduli of rGO/ANF nanocomposites. *Acta Mech.* **230**, 265–280 (2019)

18. Weng, G.J.: A dynamical theory for the Mori–Tanaka and Ponte Castañeda–Willis estimates. *Mech. Mater.* **42**, 886–893 (2010)
19. Hashin, Z., Shtrikman, S.: A variational approach to the theory of the elastic behaviour of polycrystals. *J. Mech. Phys. Solids* **10**, 343–352 (1962)
20. Nan, C.W., Birringer, R., Clarke, D.R., Gleiter, H.: Effective thermal conductivity of particulate composites with interfacial thermal resistance. *J. Appl. Phys.* **81**, 6692–6699 (1997)
21. Duan, H.L., Karihaloo, B.L., Wang, J., Yi, X.: Effective conductivities of heterogeneous media containing multiple inclusions with various spatial distributions. *Phys. Rev. B* **73**, 174203 (2006)
22. Xia, X.D., Su, Y., Zhong, Z., Weng, G.J.: A unified theory of plasticity, progressive damage and failure in graphene–metal nanocomposites. *Int. J. Plast.* **99**, 58–80 (2017)
23. Xia, X.D., Wang, Y., Zhong, Z., Weng, G.J.: Theory of electric creep and electromechanical coupling with domain evolution for non-poled and fully poled ferroelectric ceramics. *Proc. R. Soc. Lond. A* **472**, 20160468 (2016)
24. Bao, W.S., Meguid, S.A., Zhu, Z.H., Weng, G.J.: Tunneling resistance and its effect on the electrical conductivity of carbon nanotube nanocomposites. *J. Appl. Phys.* **111**, 093726 (2012)
25. Maxwell, J.C.: *A Treatise on Electricity and Magnetism*, 3rd edn. Clarendon Press, Oxford (1982)
26. Wagner, K.W.: The after effect in dielectrics. *Arch. Electrotech.* **2**, 378–394 (1914)
27. Sillars, R.W.: The properties of a dielectric containing semiconducting particles of various shapes. *Inst. Electr. Eng. Proc. Wirel. Sect.* **12**, 139–155 (1937)
28. Cao, W.Q., Wang, X.X., Yuan, J.: Temperature dependent microwave absorption of ultrathin graphene composites. *J. Mater. Chem. C* **3**, 10017–10022 (2010)
29. Yuan, J.K., Yao, S.H., Dang, Z.M., Sylvestre, A., Genestoux, M., Bai, J.B.: Giant dielectric permittivity nanocomposites: realizing true potential of pristine carbon nanotubes in Polyvinylidene Fluoride matrix through an enhanced interfacial interaction. *J. Phys. Chem. C* **115**, 5515–5521 (2011)
30. Wu, H., Liu, G., Wang, J.: Atomistic and continuum simulation on extension behaviour of single crystal with nano-holes. *Model. Simul. Mater. Sci. Eng.* **12**, 225–233 (2004)
31. Ponte Castañeda, P., Willis, J.R.: The effect of spatial distribution on the effective behavior of composite materials and cracked media. *J. Mech. Phys. Solids* **43**, 1919–1951 (1995)
32. Mori, T., Tanaka, K.: Average stress in matrix and average elastic energy of materials with misfitting inclusions. *Acta Metall.* **21**, 571–574 (1973)
33. Bruggeman, D.A.G.: Calculation of various physics constants in heterogenous substances I: dielectricity constants and conductivity of mixed bodies from isotropic substances. *Ann. Phys.* **24**, 636–664 (1935)
34. Weng, G.J.: Explicit evaluation of Willis’ bounds with ellipsoidal inclusions. *Int. J. Eng. Sci.* **30**, 83–92 (1992)
35. Eshelby, J.D.: The determination of the elastic field of an ellipsoidal inclusion, and related problems. *Proc. R. Soc. Lond. A* **241**, 376–396 (1957)
36. Švorčík, V., Králová, J., Rybka, V., Plešek, J., Červená, J., Hnatowicz, V.: Temperature dependence of the permittivity of polymer composites. *J. Polym. Sci. B* **39**, 831–834 (2001)
37. Hyun, J.G., Lee, S.Y., Cho, S.D., Paik, K.W.: Frequency and temperature dependence of dielectric constant of epoxy/BaTiO₃ composite embedded capacitor films (ECFs) for organic substrate. In: *Electronic Components and Technology Conference*. pp. 1241–1247 (2005)
38. Cao, M.S., Song, W.L., Hou, Z.L., Wen, B., Yuan, J.: The effects of temperature and frequency on the dielectric properties, electromagnetic interference shielding and microwave-absorption of short carbon fiber/silica composites. *Carbon* **48**, 788–796 (2010)
39. Bolotin, K.I., Sikes, K.J., Hone, J., Stormer, H.L., Kim, P.: Temperature-dependent transport in suspended graphene. *Phys. Rev. Lett.* **101**, 096802 (2008)
40. Huang, X., Zhi, C., Jiang, P., Golberg, D., Bando, Y., Tanaka, T.: Temperature-dependent electrical property transition of graphene oxide paper. *Nanotechnology* **23**, 455705 (2012)
41. Li, J., Weng, G.J.: A theory of domain switch for the nonlinear behaviour of ferroelectrics. *Proc. R. Soc. Lond. A* **455**, 3493–3511 (1999)
42. Landau, L.D.: On the theory of phase transitions. I. *Zh. Eksp. Teor. Fiz.* **11**, 19–42 (1937)
43. Ginzburg, V.L.: The dielectric properties of crystals of seignetteelectric substances and of barium titanate. *Zh. Eksp. Teor. Fiz.* **15**, 739–749 (1945)
44. Su, Y., Weng, G.J.: The frequency dependence of microstructure evolution in a ferroelectric nano-film during AC dynamic polarization switching. *Acta Mech.* **229**, 795–805 (2018)
45. Wang, Y., Weng, G.J., Meguid, S.A., Hamouda, A.M.: A continuum model with a percolation threshold and tunneling-assisted interfacial conductivity for carbon nanotube-based nanocomposites. *J. Appl. Phys.* **115**, 193706 (2014)
46. Chen, Z., Xu, C., Ma, C., Ren, W., Cheng, H.M.: Lightweight and flexible graphene foam composites for high-performance electromagnetic interference shielding. *Adv. Mater.* **25**, 1296–1300 (2013)
47. Mohiuddin, M., Hoa, S.V.: Temperature dependent electrical conductivity of CNT-PEEK composites. *Compos. Sci. Technol.* **72**, 21–27 (2011)
48. Ramanathan, T., Abdala, A.A., Stankovich, S., Dikin, D.A., Herrera-Alonso, M., Piner, R.D., Adamson, D.H., Schniepp, H.C., Chen, X., Ruoff, R.S., Nguyen, S.T., Aksay, I.A., Prud’homme, R.K., Brinson, L.C.: Functionalized graphene sheets for polymer nanocomposites. *Nat. Nanotech.* **3**, 327–331 (2008)